Applied Physics B (2020) 126:35
https://doi.org/10.1007/s00340-020-7386-6

Applied Physics B
Lasers and Optics

Goos–Hänchen shift for elegant Hermite–Gauss light beams impinging on dielectric surfaces coated with a monolayer of graphene

Weiming Zhen[1] · **Dongmei Deng**[1]

Received: 2 December 2019 / Accepted: 23 January 2020 / Published online: 8 February 2020

Abstract
The Goos–Hänchen (GH) shift for the reflection of the elegant Hermite–Gauss beams (EHGBs) impinging on single-layer graphene-coated surfaces is theoretically studied. The factors influencing the GH shift, including the incident angle, the refractive index and the orders m and n of H_{mn} EHGBs are analyzed, respectively. It is shown that with the increase of the order m, the variations of the GH shift of different EHGBs are greatly enhanced. Thus, the GH shift of the EHGBs can be manipulated by choosing the order m.

1 Introduction

In the wave optics, as we all know, the reflected and refractive beams of light exhibited by plane electromagnetic waves through a surface are governed by Fresnel equations and Snell' law [1]. To the physical beams, however, there are many non-specular reflection phenomena, and the most important ones are the Goos–Hänchen (GH) [2–5] and Imbert–Fedorov (IF) [6, 7] shifts, occurring in the incident plane of light and the plane perpendicular to the plane of incidence, respectively. The effect of the GH shift was predicted and observed experimentally by Goos and Hänchen [2–4]. Artmann explained that for the bound beam, various phase changes leaded to the GH shift and he derived Artmann formula [5]. The GH shift can be studied at the surface of various media [8–11]. Moreover, the GH shift of the polarized Gaussian beam by a moving object was investigated [12]. These shifts have applications in many diverse fields [13–21]. In 2007, Li [22] established an unified theory for GH and IF shifts using the two-form amplitude. Aiello and Woerdman derived the function expression for the GH and IF shifts by studying role of beam propagation [23] and then they also presented a theory of angular GH shift near Brewster incidence [24]. Aiello proposed a new method to theoretically calculate these shifts [25]. At the critical angle, a new analytic expression for the GH shift was derived [26].

Recently, there are many investigations of the GH shift for different beam shapes, including Hermite–Gaussian [27, 28], Laguerre–Gaussian [29, 30], Hermite–Laguerre–Gaussian [31, 32], astigmatic Gaussian [33], Bessel [34], Airy [35–37] and vortex beams [38, 39] etc.

The elegant Hermite–Gaussian beams (EHGBs), the solutions of the paraxial wave equation, were introduced by Siegman, which are not orthogonal in the usual sense and the argument of the Hermite part is complex [40]. Saghafi et al. investigated the near- and far-field behaviors of the elegant Hermite Gaussian modes [41]. We have studied coherent and incoherent combinations of EHGBs [42], investigated analytically and numerically the propagation of elegant Hermite cosine Gaussian laser beams [43], and derived the first three orders of nonparaxial corrections for the elegant Hermite–Laguerre–Gaussian beams [44].

On the other hand, graphene, as a two-dimensional (2D) semiconductor, captured wide attention in recent years, due to its unique optical and electronic properties [45–47]. In recent decade, the GH shift in graphene-containing structures was studied widely, thanks to the appearance of the giant GH shift [48], which also provided the method of controlling the GH shift by changing the external voltage. And then, under a total internal reflection condition, the giant GH shift was originally observed and proved experimentally [49]. Grosche et al. [50] studied a theoretical calculation of a systematical and numerical analysis of the GH and IF shifts for Gaussian beams impinging on a monolayer graphene-coated surface. The GH shift of light beams impinging on a

✉ Dongmei Deng
dmdeng@263.net

[1] Guangdong Provincial Key Laboratory of Nanophotonic Functional Materials and Devices, South China Normal University, Guangzhou 510631, China

single-layer graphene decreased with increasing Fermi level at higher frequencies, while the shift was directly proportional to the Fermi level at lower frequencies [51]. A giant quantized GH shift on the surface of graphene in the quantum Hall regime was theoretically investigated [52]. The GH shift in graphene was experimentally observed by weak measurements [53]. Meanwhile, lots of works on investigation of the photonic spin Hall effect (SHE) in graphene have been extensively published [54–58]. In addition, photonic SHE has many practical applications in physics. Using the quantum weak measurement techniques, the photonic SHE holds great potential for precision metrology [59], such as measuring the thickness of nanometal films [60], measuring the axion coupling of topological materials [61], and identifying the layer of graphene [54] as well as topological phase transitions [62]. The GH shift and the photonic SHE in graphene have been widely studied and applied in physics, but the GH shift for the EHGB has not been theoretically and systematically analyzed so far.

In this work, the GH shift for the EHGBs impinging on a monolayer graphene-coated surface is investigated. The rest of this paper is arranged as follows: the expression of the GH shift of the *p*- and *s*-polarized H_{mn} mode EHGBs is derived in Sect. 2. In Sect. 3, based on the analytical solution, we get the results and discussions for two cases: the beam reflection first occurs from the dielectric medium to the air, and later from the air to the dielectric medium. We conclude some useful results in Sect. 4.

2 Model and methods

We consider a monochromatic three-dimensional EHGB impinging on a dielectric surface whose refractive index is μ coated with a single layer of graphene which is described by the optical conductivity $\sigma(\Omega)$. The reflections first occurring from the dielectric medium to the air and latter from the air to the dielectric medium are studied, respectively. Figure 1 gives the schematic diagram for the GH shift of a geometry beam reflection taking place from the air to the dielectric medium. A single layer of graphene is located on the plane $x = 0$, and obviously the incident plane is $x - y$ plane.

According to Li [22], the vector electric field of the beam is expressed in terms of its vector angular spectrum as:

$$\boldsymbol{E}(x,y,z) = \frac{1}{2\pi}\int_{-\infty}^{+\infty}\int_{-\infty}^{+\infty}\boldsymbol{A}\left(k_y,k_z\right) \mathrm{e}^{i(k_y y+k_z z)}\mathrm{d}k_y\mathrm{d}k_z, \tag{1}$$

where $k = 2\pi\mu/\lambda_0$ is the wave number along with $k^2 = k_x^2 + k_y^2 + k_z^2$, where λ_0 is the wavelength in vacuum. The optical conductivity $\sigma(\Omega)$ can be given by Katsnelson [63], as follows:

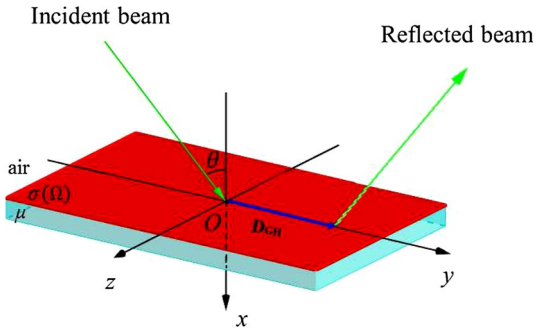

Fig. 1 Schematic diagram for the GH shift of a geometry beam reflection at the interface. A monolayer of graphene is located on the surface at $x = 0$

$$\sigma_0 = H(\Omega-2) + i\left[\frac{4}{\pi\Omega} - \frac{1}{\pi}\ln\left|\frac{\Omega+2}{\Omega-2}\right|\right], \tag{2}$$

where $\sigma_0 = \mathrm{e}^2/4\hbar = \pi\alpha c\varepsilon_0$ is the universal optical conductivity of graphene, $\Omega = \hbar\omega/\mu_G$ is the dimensionless frequency, μ_G is the chemical potential of graphene and $H(x)$ is the Heaviside step function. For simplicity, we choose $\mu = 1.5$ and $\Omega = 2.5$ by regulating μ_G as the following numerical simulation.

On the basis of Li [22], the incident beam can be expressed as two-form amplitude:

$$\tilde{A}_i = \left(l_{ip}\tilde{p} + l_{is}\tilde{s}\right) = \tilde{L}_i A, \tag{3}$$

where $\tilde{L}i = l_{ip}\tilde{p} + l_{is}\tilde{s}$ is the matrix which describes the complete state of the polarization of the incident beam, and

$$\boldsymbol{A}^{\dagger}\frac{\partial \boldsymbol{A}}{\partial k_y} = \tilde{A}^{\dagger}\frac{\partial \tilde{A}}{\partial k_y} - \frac{k_x k_y}{k\left(k_y^2+k_2^2\right)}\left(A_s^* A_p - A_p^* A_s\right). \tag{4}$$

Nowadays, we consider a monochromatic EHGB propagating in the direction of the x axis, and θ is the incident angle (Fig. 1). The angular spectrum amplitude function $A\left(k_y,k_z\right)$ can be regarded as a positive definite sharply symmetric function peaked around $\left(k_{y0},k_{z0}\right) = (k\sin\theta, 0)$. The normalized amplitude spectrum function of the EHGB is:

$$\begin{aligned} A\left(k_y,k_z\right) =& (-1)^{m+n}\sqrt{\frac{w_y w_z}{2^{m+n+1}\Gamma\left(m+\frac{1}{2}\right)\Gamma\left(n+\frac{1}{2}\right)\pi}} \\ & \left[\left(k_y-k_{y0}\right)w_y\right]^m \\ & \times\left(k_z w_z\right)^n \exp\left[-\frac{\left(k_y-k_{y0}\right)^2 w_y^2}{4}\right] \\ & \exp\left(-\frac{k_z^2 w_z^2}{4}\right), \end{aligned} \tag{5}$$

where $\Gamma(x)$ is the gamma function, is the half width of the EHGB at waist. Especially, when the orders m and n both are 0, Eq. (5) becomes the case of the fundamental Gaussian beam.

In the study of the GH shift, we consider the p- and s-polarized EHGBs, whose complete states of the polarization are $\tilde{L}i = \begin{pmatrix} 1 \\ 0 \end{pmatrix}$ and $\tilde{L}i = \begin{pmatrix} 0 \\ 1 \end{pmatrix}$, respectively. For the incident beam,

$$A_s^* A_p - A_p^* A_s = 0. \tag{6}$$

We are grounded on Li [22], on the xoz plane, the y coordinate of the centroid of the incident beam satisfies

$$\langle y_i \rangle = 0. \tag{7}$$

And we know that the GH shift is $D_{GHj} = \langle y_r \rangle - \langle y_i \rangle$, so we obtain the GH shift for the p- or s- polarized beams

$$D_{GHj} = \langle y_r \rangle - \langle y_i \rangle = -\frac{1}{Q_j} \int_{-\infty}^{+\infty} \int_{-\infty}^{+\infty} \left|R_j\right|^2 |A|^2 \frac{\partial \phi_j}{\partial k_y} \mathrm{d}k_y \mathrm{d}k_z, \tag{8}$$

where $Q_j = \int_{-\infty}^{+\infty} \int_{-\infty}^{+\infty} \left|R_j\right|^2 |A|^2 \mathrm{d}k_y \mathrm{d}k_z$, $\left|R_j\right|$ is the reflective coefficient for the p- or s- polarized beam, phase ϕ_j is given by $R_j = \left|R_j\right| \exp\left(i\phi_j\right)$, and $j = p$ or s.

In quantitative estimates, we use a wavelength λ_0 =634 nm, half of waist $w_0 = 2.5\,\mu$m, p- and s-polarized EHGBs incident with the centroid at the origin, and the taken values of $\tilde{L}i$ above for the study of the GH shift. As calculating Eq. (8), we need to use the relation $k_y^2 + k_z^2 = k^2 - k_x^2 = k^2 \cos^2\theta$. We calculate the GH shift of the reflection beams using Wolfram Mathematica on the computer.

3 Results and discussions

In the former case, the reflection takes place from the dielectric medium (at refractive index μ to the air. According to the Ref. [64], the Fresnel reflection coefficients of a single layer of graphene deposited on the dielectric surface are provided by

$$R_p(\theta) = \frac{\cos\theta - \mu\sqrt{1-\mu^2\sin^2\theta}\left[1 - \sigma(\Omega)\cos\theta/c\varepsilon_0\right]}{\cos\theta + \mu\sqrt{1-\mu^2\sin^2\theta}\left[1 + \sigma(\Omega)\cos\theta/c\varepsilon_0\right]},$$
$$R_s(\theta) = \frac{\mu\cos\theta - \sqrt{1-\mu^2\sin^2\theta} - \mu\sigma(\Omega)/c\varepsilon_0}{\mu\cos\theta + \sqrt{1-\mu^2\sin^2\theta} + \mu\sigma(\Omega)/c\varepsilon_0}. \tag{9}$$

In the latter case, the reflection taking place from the air to the dielectric medium can also be considered. The Fresnel reflection coefficients given by Eq. (9) are changed into [64]:

$$R_p(\theta) = \frac{\mu^2\cos\theta - \sqrt{\mu^2-\sin^2\theta}\left[1 - \sigma(\Omega)\cos\theta/c\varepsilon_0\right]}{\mu^2\cos\theta + \sqrt{\mu^2-\sin^2\theta}\left[1 + \sigma(\Omega)\cos\theta/c\varepsilon_0\right]},$$
$$R_s(\theta) = \frac{\cos\theta - \sqrt{\mu^2-\sin^2\theta} - \sigma(\Omega)/c\varepsilon_0}{\cos\theta + \sqrt{\mu^2-\sin^2\theta} + \sigma(\Omega)/c\varepsilon_0}. \tag{10}$$

The calculations of the GH shift for the p- and s-polarized EHGBs are simulated, respectively.

3.1 The GH shift for the *p*-polarized EHGBs

Figure 2 shows the GH shift for the p-polarized EHGBs of H_{10}, H_{01}, H_{20} and H_{02} (a) and (c), H_{30}, H_{03}, H_{22} and H_{33} (b) and (d); the reflection takes place from the dielectric medium to the air (a) and (b) and from the air to the dielectric medium (c) and (d), all with the angle of incidence θ at $\mu = 1.5$. The curves of Fig. 2a, b nearly coincide. Beginning from 33.8°, the GH shift for p-polarization slowly increases from near zero with the increasing angle of incidence up to the Brewster angle $\theta_B = 33.69°$. Next, the GH shift decreases sharply and a negative valley appears at $\theta = 34.08°$ and the shift is a negative value. We know that the minus sign represents the negative direction of the y-axis. Afterwards, the GH shift increases very rapidly to another large positive peak again. The above two positive peaks occur at $\theta = 33.95°$ and $\theta = 34.20°$ individually. Subsequently, the GH shift reduces

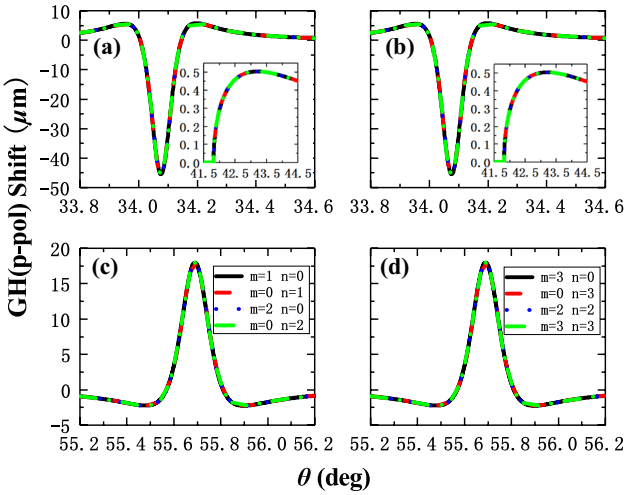

Fig. 2 The GH shift of the reflection taking place from the dielectric medium ($\mu = 1.5$) to the air (**a**) and (**b**), from the air to the dielectric medium ($\mu = 1.5$) (**c**) and (**d**) for the p-polarized EHGBs of (**a**) and (**c**) H_{10}, H_{01}, H_{20} and H_{02}, **b** and **d** H_{30}, H_{03}, H_{22} and H_{33}; all with the incident angle θ

to zero. Near the critical angle $\theta_c = 41.81°$, the GH shift increases again. At $\theta = 43.02°$, the GH shift arrives at an extremely small and positive peak, and then it starts reducing quickly to zero again with the increasing θ. The reason why this obvious variety observed near the Brewster angle is that the phase of the reflection coefficient ϕ_p changes very rapidly from the π to 0 on about θ_B [50]. This leads to a pair of relatively large and positive GH shifts and a negative peak shift whose absolute value arrives at the maximum. Near θ_c, the reflected wave goes along the reflected surface with the lack of any obstacle, satisfying the momentum balance equation [28], so the GH shift can also arrive at a small peak. Obviously, the variations of these GH shifts are so much bigger near θ_B than the ones near θ_c, namely, the sensitivity of variations of the GH shifts values to the Brewster angle is much stronger than the one to the critical angle. In Fig. 2c, d, all the curves are nearly coinciding. In this case, despite it has no total internal reflection, the GH shift also exists, due to the nonzero slope of the reflection coefficient ϕ_s. θ starts from 55.2°, the GH shift is about zero and the shift has no obvious variation. Near the Brewster angle $\theta_B = 56.31°$, the GH shift firstly decreases to a negative valley and then increases strongly to a positive peak. The GH shift arrives at a relatively large and positive value at $\theta = 55.69°$. And then, the GH shift decreases again to another negative valley. The above two negative valleys appear at $\theta = 55.48°$ and $\theta = 55.90°$, respectively. After that, the GH shift increases sharply to zero with the increasing θ. The reason why the GH shift has a positive maximum value near θ_B is analogous to the first case: the phase ϕ_s changes so violently from the θ to $-\pi$ [50].

Figure 3 shows the GH shift for the p-polarized EHGBs of H_{10}, H_{01}, H_{20} and H_{02} (a) and (c), H_{30}, H_{03}, H_{22} and H_{33} (b) and (d); the reflection takes place from the dielectric medium to the air at $\theta = 42°$ (a) and (b), and from the air to the dielectric medium at $\theta = 56.5°$ (c) and (d), all with the refractive index μ. In Fig. 3a, b, all the curves nearly coincide. Staring from μ =1.13, the GH shift for p-polarization increases up to μ for which $\theta = 42°$ corresponds to near θ_B of the medium. The first positive peak occurs at $\mu = 1.149$ and then the GH shift decreases sharply to the negative value up to $\mu = 1.162$, where a maximal absolute value of the GH shift appears. It immediately increases again to another positive peak at $\mu = 1.174$, and then decreases until μ for which $\theta = 42°$ corresponds to near θ_c. A relative small and positive GH shift appears at $\mu = 1.539$. After that, the GH shift decreases quickly to zero with increasing μ. In practice, to obtain the low refractive indexes range from 1.13 to 1.23, we can use the silica aerogels as the dielectric media, which have many properties, including low density, low thermal conductivity, large surface area and high porosity [65], and have lots of applications, such as in chemistry [66] and in catalysis [67], whose refractive index of 1.14–1.16 can be

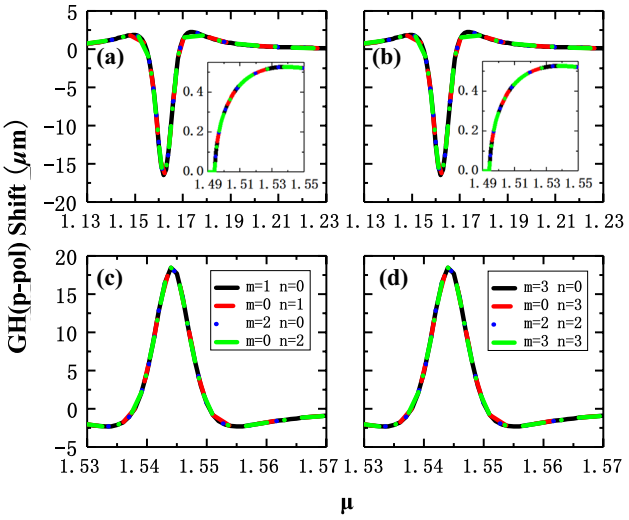

Fig. 3 The GH shift of the reflection taking place from the dielectric medium to the air at $\theta = 42°$ (**a**) and (**b**), and from the air to the dielectric medium at $\theta = 56.5°$ (**c**) and (**d**), for the p-polarized EHGBs of (**a**) and (**c**) H_{10}, H_{01}, H_{20} and H_{02}, **b** and **d** H_{30}, H_{03}, H_{22} and H_{33}; all with the refractive index μ of the dielectric medium

gained by controlling relative humidity [68]. In Fig. 3c, d, all curves are also nearly coincident. Beginning from $\mu = 1.53$, the GH shift is nearby zero and has little clear variation up to μ for which $\theta = 56.5°$ corresponds to near θ_B of the medium. The GH shift decreases to a negative valley at $\mu = 1.533$. And then, the GH shift increases strongly to a maximal and positive value at $\mu = 1.544$. Next, the second negative valley occurs at $\mu = 1.555$. Finally, the GH shift increases sharply to zero as μ increases. Note that the consequences from Fig. 3 are consistent with ones in Fig. 2.

Figure 4 shows the variation of the GH shift for the p-polarized EHGBs of (a) and (c) $H_{mn}(m = n = N, N = 0,1,2,3)$, (b) and (d) H_{m0} $(m = N, N = 1,2,3)$ and H_{0n} $(n = N, N = 1,2,3)$ with the order N; the reflection takes place from the dielectric medium to the air at $\theta = 55.69°$(a) and (b), and from the air to the dielectric medium at $\theta = 34.08°$ (c) and (d); all at $\mu = 1.5$. Whenever in Fig. 4a, b or in the Fig. 4c, d, the dots, which represent the GH shifts, nearly coincide with the order N varying from 0 to 2, respectively. In the former cases (a) and (b), the dots on the H_{30} and H_{33} beams are larger evidently than the others; while in the latter cases (c) and (d), the dots representing the types H_{30} and H_{33} beams are smaller obviously than the others. Though it seems that the orders m and n of H_{mn} of the EHGBs have little influence on the GH shift for p-polarization in Figs. 2 and 3, actually, the significances of the orders m and n of the H_{mn} are asymmetric. The changes of the magnitude of the GH shift are more obvious by varying the value of m than that by varying the value of n, namely, the dependence of the GH shift value on m is stronger than the one on n. Although the dots on H_{00},

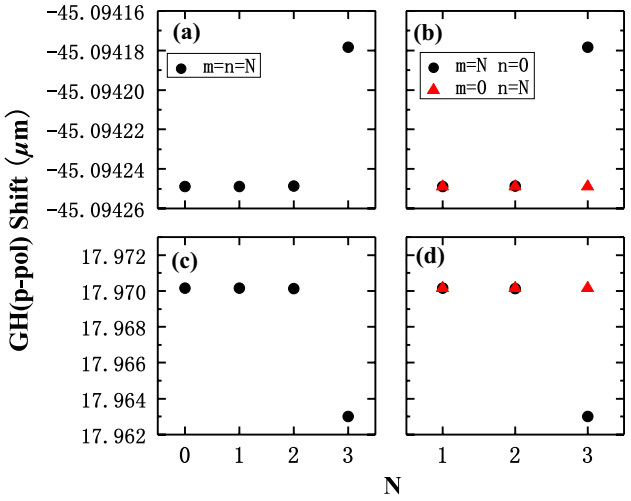

Fig. 4 The GH shift of the reflection taking place from the dielectric medium ($\mu = 1.5$) to the air at $\theta = 55.69°$ (**a**) and (**b**), and from the air to the dielectric medium ($\mu = 1.5$) at $\theta = 34.08°$ (**c**) and (**d**), for the *p*-polarized EHGBs of (**a**) and (**c**) $H_{mn}(m = n = N, N = 0,1,2,3)$, **b** and **d** H_{m0} ($m = N, N = 1,2,3$) and H_{0n} ($n = N, N = 1,2,3$) with the order N

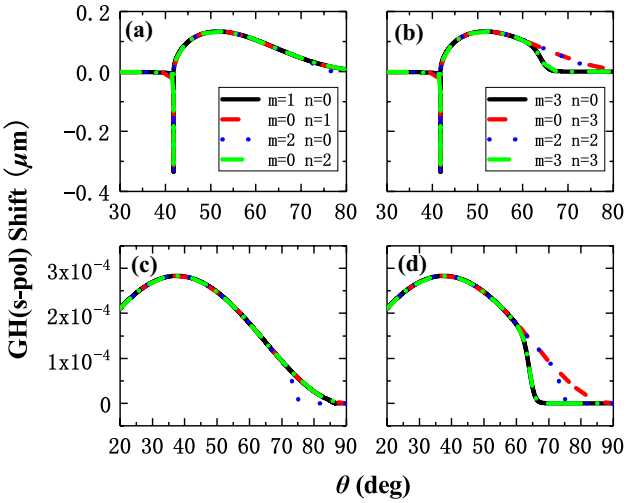

Fig. 5 The GH shift of the reflection taking place from the dielectric medium (the refractive index $\mu = 1.5$) to the air (**a**) and (**b**), from the air to the dielectric medium (the refractive index $\mu = 1.5$) (**c**) and (**d**) for the *s*-polarized EHGBs of (**a**) and (**c**) H_{10}, H_{01}, H_{20} and H_{02}, **b** and **d** H_{30}, H_{03}, H_{22} and H_{33}; all with the incident angle θ

H_{10}, H_{01}, H_{20}, H_{02}, H_{11} and H_{22} are consistent nearly, the differences from those dots are too small to be seen. Only when the order N is bigger, the differences of the GH shifts between m and n of the type H_{mn} are bigger and more obvious. Therefore, in the former case, the change of m at $\theta = 55.69°$ can control the GH shift; while in the latter case, the change of m at $\theta = 34.08°$ can also control the GH shift.

3.2 The GH shift for the *s*-polarized EHGBs

Figure 5 shows the GH shift for the *s*-polarized EHGBs of H_{10}, H_{01}, H_{20} and H_{02} (a) and (c), H_{30}, H_{03}, H_{22} and H_{33} (b) and (d); the reflection takes place from the dielectric medium to the air (a) and (b) and from the air to the dielectric medium (c) and (d), all with the angle of incidence θ at $\mu = 1.5$. In Fig. 5a, b, not all the curves are totally coincident. Starting from 30°, the GH shift for *s*-polarization is near zero and has little variation with the increasing incident angle θ until the critical angle $\theta_c = 41.81°$, where the maximum of the absolute value of the GH shift appears. This shift value is negative. After, the GH shift increases as θ increases, and the positive maximal GH shift occurs at $\theta = 51.66°$. So far all the curves in Fig. 5a, b coincide. After that, however, the differences of different curves appear. The GH shifts of H_{10}, H_{01}, H_{02} and H_{03} beams decrease monotonically with the increasing θ and then tend to zero. The GH shifts of H_{20} and H_{22} decrease as θ increases, and especially near $\theta = 71.91°$ these shifts decrease more quickly than the ones of H_{10}, H_{01}, H_{02} and H_{03} beams. Similarly, the GH shifts of H_{30} and H_{33} beams decrease more quickly than the ones of the others when θ is about 61.64°. In the latter case (Fig. 5c, d), beginning from 20°, the GH shifts increase with the increasing θ up to 37.55° where the only one positive maximal GH shift appears. And then, the GH shifts decrease as θ increases; meanwhile, there are differences among the GH shifts of various H_{mn} beams. As the former case, near $\theta = 71.79°$, the GH shifts of H_{20} and H_{22} beams decrease more quickly than the ones of H_{10}, H_{01}, H_{02} and H_{03} beams; and near $\theta = 61.64°$, the GH shifts of H_{30} and H_{33} beams decrease more quickly than the ones of the others. Whenever in the former case or in the latter case, the bigger the order m is, the quicker and earlier decreases the GH shift near the grazing angle. For the *s*-polarized EHGBs, the θ_B has little impact on the GH shift, which is different from the case for the *p*-polarized beams.

Figure 6 shows the GH shift for the *s*-polarized EHGBs of H_{10}, H_{01}, H_{20} and H_{02} (a) and (c), H_{30}, H_{03}, H_{22} and H_{33} (b) and (d); the reflection takes place from the dielectric medium to the air at $\theta = 42°$ (a) and (b), and from the air to the dielectric medium at $\theta = 56.5°$ (c) and (d), all with the refractive index μ. Whenever in the former case (Fig. 6a, b) or in the latter case (Fig. 6c, d), all curves are nearly coincident. In the former case, starting from $\mu = 1.4$, the GH shift increases from a negative value as μ increases. At $\mu = 1.485$, the GH shift begins to decrease strongly until $\mu = 1.494$ for which $\theta = 42°$ corresponds to near θ_c. There is the maximal absolute value of the GH shift whose value is negative. And then, the GH shift increases again with increasing μ up to 1.735, where a positive maximal shift appears. After, the GH shift monotonically decreases as μ increases. In the latter case,

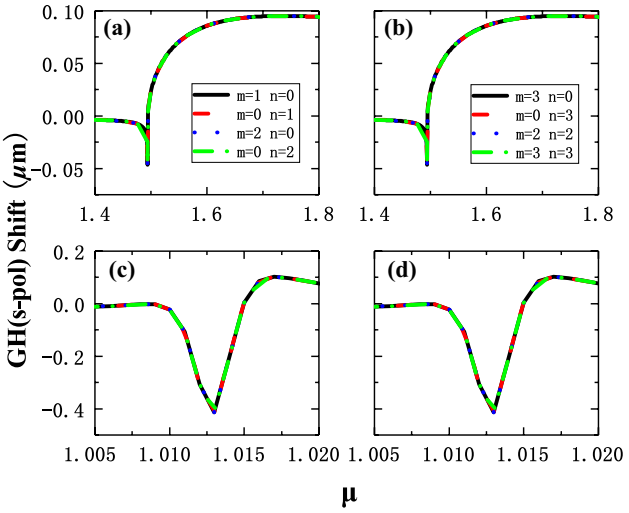

Fig. 6 The GH shift of the reflection taking place from the dielectric medium to the air at $\theta = 42°$ (**a**) and (**b**), and from the air to the dielectric medium at $\theta = 56.5°$ (**c**) and (**d**), for the *s*-polarized EHGBs of (**a**) and (**c**) H_{10}, H_{01}, H_{20} and H_{02}, **b** and **d** H_{30}, H_{03}, H_{22} and H_{33}; all with the refractive index μ of the dielectric medium

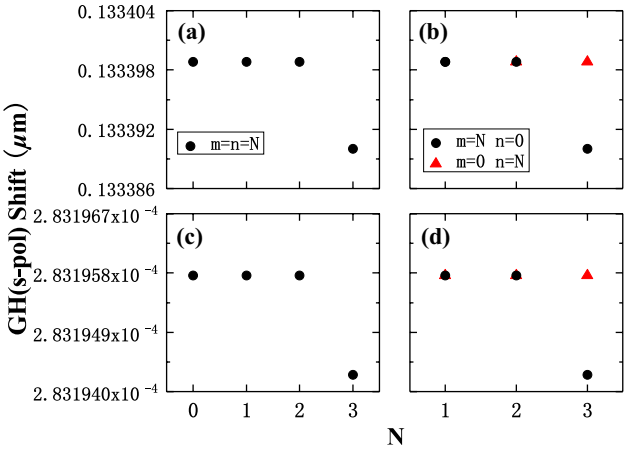

Fig. 7 The GH shift of the reflection taking place from the dielectric medium ($\mu = 1.5$) to the air at $\theta = 51.66°$ (**a**) and (**b**), and from the air to the dielectric medium ($\mu = 1.5$) at $\theta = 37.55°$ (**c**) and (**d**), for the *s*-polarized EHGBs of (**a**) and (**c**) $H_{mn}(m = n = N, N = 0,1,2,3)$, **b** and **d** H_{m0} ($m = N, N = 1,2,3$) and H_{0n} ($n = N, N = 1,2,3$) with the order N

the GH shift decreases strongly form a negative value until $\mu = 1.013$, where a maximal absolute value of shift appears and this value is negative. After, the GH shift increases quickly with the increase of μ. When $\mu = 1.017$, the GH shift arrives at the only positive maximum. Afterwards, the GH shift decreases sharply to zero with μ. In this case, the silica aerogels with $\mu = 1.013$ can be produced by Adachi et al. [69]. Therefore, the silica aerogels can be regarded as the dielectric media to generate a large and negative GH shift.

Figure 7 shows the variation of the GH shift for the *s*-polarized EHGBs of (a) and (c) $H_{mn}(m = n = N, N = 0,1,2,3)$, (b) and (d) $H_{m0}(m = N, N = 1,2,3)$ and $H_{0n}(n = N, N = 1,2,3)$ with the order N; the reflection takes place from the dielectric medium to the air at $\theta = 51.66°$ (a) and (b), and from the air to the dielectric medium at $\theta = 37.55°$ (c) and (d); all at $\mu = 1.5$. Whenever in Fig. 7a, b or in Fig. 7c, d, the dots, which represent the GH shifts, nearly coincide with the order N varying from 0 to 2, respectively. Similar to the GH shift for *p*-polarization (Fig. 4), the dots on the H_{30} and H_{33} beams are smaller evidently than the others. It means that the influence to the GH shift for *s*-polarization on the orders m and n of H_{mn} beams is asymmetric. However, the differences from the dots on the H_{00}, H_{10}, H_{01}, H_{20}, H_{02}, H_{11} and H_{22} are too small to be seen. When the order N is higher, the differences of the GH shifts between m and n of the H_{mn} beams are bigger and more obvious. It is more obvious that the differences of the magnitudes of GH shifts occur, when the order m, rather than n, is changed. Therefore, the dependence of the GH shift on the order m is bigger than the one on the order n.

4 Conclusion

In this paper, the GH shift for the H_{mn} mode of the EHGBs impinging on the dielectric surfaces (whose the refractive index is μ) coated with a monolayer of graphene is studied. The factors which influence the GH shift, including the incident angle, the refractive index and the orders m and n of the EHGBs are analyzed, respectively. In particular, the dependencies of this shift on the Brewster angle and the critical angle are discussed. These aspects were investigated theoretically by Aiello et al. in 2009 [24] and by Araújo et al. in 2016 [26], respectively, but they studied the GH shift of the reflected Gaussian beam from air–dielectric surfaces. Due to graphene deposited on the dielectric and the EHGBs, our results are some differences from them. We find that the GH shift of the *p*-polarized EHGB at near the Brewster angle θ_B is much larger than the one at near the critical angle θ_c, namely the dependence of the variation of the GH shift on about θ_B is more superior to the one on about θ_c. For an *s*-polarized EHGB, however, the Brewster angle θ_B has no any influence on the GH shift. In total internal reflection region, there is the maximum value of the GH shift for a *p*-polarized EHGB at the incident angle greater than θ_c. This special angle, however, does not satisfy Eq. (20) in Ref. [26]. The GH shift in graphene-coated surfaces was firstly studied by Grosche et al. [50]. Compared with this, we not only consider the EHGBs as the incoming light, but also use Li's theory to calculate the GH shift [22]. Despite they have investigated the shift for the case with TIR (reflection taking place from the dielectric medium to the air), the Brewster angle was not considered. In this case, we find that, there is a big and negative GH shift near θ_B both in

the *p*- or *s*-polarized beams. Moreover, for the case of the reflection taking place from the air to dielectric, the maximal shift appears in 37.55° instead of 90°, which is different from the result in Ref. [50]. Therefore, our study expands our knowledge for the GH shift in graphene. Notably, the influences of the orders *m* and *n* of the H_{mn} beams are asymmetric, and the variations of the GH shift among the different orders are relatively obvious as *m*, rather than *n*, is changed. Furthermore, with the increase of the order *m*, theses variations of the GH shift are greatly enhanced. In a word, we can control the values of the GH shift by changing appropriately the order m of H_{mn} EHGBs at a specific incident angle. There is also the primal numerical simulation of the GH shift of the reflection of the EHGBs impinging upon a single layer of graphene-coated surfaces.

Acknowledgements National Natural Science Foundation of China (11775083 and 11374108).

References

1. M. Born, E. Wolf, *Principles of Optics* (Cambridge University Press, Cambridge, 2003)
2. F. Goos, H. Hänchen, Ann. Phys. **435**, 383–392 (1943)
3. F. Goos, H. Hänchen, Ann. Phys. **436**, 333–346 (1947)
4. F. Goos, H. Lindberg-Hänchen, Ann. Phys. **440**, 251–252 (1949)
5. K. Artmann, Ann. Phys. **437**, 87–102 (1948)
6. C. Imbert, Phys. Rev. D **5**, 787–796 (1972)
7. F.I. Fedorov, Dokl. Akad. Nauk SSSR **105**, 465–467 (1955)
8. C. Luo, J. Guo, Q. Wang, Y. Xiang, S. Wen, Opt. Express **21**, 10430–10439 (2013)
9. F. Liu, J. Xu, G. Song, Y. Yang, J. Opt. Soc. Am. B **30**, 1167–1172 (2013)
10. I.V. Shadrivov, A.A. Zharov, Y.S. Kivshar, Appl. Phys. Lett. **83**, 2713–2715 (2003)
11. Y. Xu, C.T. Chan, H. Chen, Sci. Rep. **5**, 8681 (2015)
12. H. Wang, X. Zhang, J. Opt. Soc. Am. B **29**, 1218–1225 (2012)
13. O. Emile, T. Galstyan, A. Le Floch, F. Bretenaker, Phys. Rev. Lett. **75**, 1511–1513 (1995)
14. B.M. Jost, A.-A.R. Al-Rashed, B.E.A. Saleh, Phys. Rev. Lett. **81**, 2233–2235 (1998)
15. J. Huang, Z. Duan, H.Y. Ling, W. Zhang, Phys. Rev. A **77**, 063608 (2008)
16. R. Briers, O. Leroy, G. Shkerdin, J. Acoust. Soc. Am. **108**, 1622–1630 (2000)
17. X. Yin, L. Hesselink, Z. Liu, N. Fang, X. Zhang, Appl. Phys. Lett. **85**, 372–374 (2004)
18. A. Farmani, M. Miri, M.H. Sheikhi, J. Opt. Soc. Am. B **34**, 1097–1106 (2017)
19. R.H. Renard, J. Opt. Soc. Am. **54**, 1190–1197 (1964)
20. V.K. Ignatovich, Phys. Lett. A **322**, 36–46 (2004)
21. C.W.J. Beenakker, R.A. Sepkhanov, A.R. Akhmerov, J. Tworzydło, Phys. Rev. Lett. **102**, 146804 (2009)
22. C.-F. Li, Phys. Lett. A **76**, 013811 (2007)
23. A. Aiello, J.P. Woerdman, Opt. Lett. **33**, 1437–1439 (2008)
24. A. Aiello, J. P. Woerdman, arXiv:0903.3730v2 (2009)
25. A. Aiello, New J. Phys. **14**, 013058 (2012)
26. M.P. Araújo, Stefano De Leo, G.G. Maia, Phys. Rev. A **93**, 023801 (2016)
27. D. Golla, S.D. Gupta, Pramana **76**, 603–612 (2011)
28. C. Prajapati, D. Ranganathan, J. Opt. Soc. Am. A **29**, 1377–1382 (2012)
29. K.N. Pichugin, D.N. Maksimov, A.F. Sadreev, J. Opt. Soc. Am. A **35**, 1324–1329 (2018)
30. X. Guo, X. Liu, W. Zhu, M. Gao, W. Long, J. Yu, H. Zheng, H. Guan, Y. Luo, H. Lu, J. Zhang, Z. Chen, Opt. Commun. **445**, 5–9 (2019)
31. A.M. Nugrowati, W.G. Stam, J.P. Woerdman, Opt. Express **20**, 27429–27441 (2012)
32. A.M. Nugrowati, J.P. Woerdman, Opt. Commun. **308**, 253–255 (2013)
33. M. Ornigotti, A. Aiello, J. Opt. **17**, 065608 (2015)
34. A. Aiello, J.P. Woerdman, Opt. Lett. **36**, 543–545 (2011)
35. P. Chamorro-Posada, J. Sánchez-Curto, A.B. Aceves, G.S. McDonald, Opt. Lett. **39**, 1378–1381 (2014)
36. M. Ornigotti, Opt. Lett. **43**, 1411–1414 (2018)
37. C. Zhai, S. Zhang, Optik **184**, 234–240 (2019)
38. K.Y. Bliokh, I.V. Shadrivov, Y.S. Kivshar, Opt. Lett. **34**, 389–391 (2009)
39. Z. Xiao, H. Luo, S. Wen, Phys. Rev. A **85**, 053822 (2012)
40. A.E. Siegman, J. Opt. Soc. Am. **63**, 1093–1094 (1973)
41. S. Saghafi, C.J.R. Sheppard, J. Mod. Opt. **45**, 1999–2009 (1998)
42. D. Deng, H. Guo, X. Chen, H.J. Kong, J. Opt. A-Pure Appl. Opt. **5**, 489–494 (2003)
43. D. Deng, Opt. Commun. **259**, 409–414 (2006)
44. D. Deng, Q. Guo, Opt. Lett. **33**, 1225–1227 (2008)
45. L.A. Falkovsky, J. Phys. Conf. Ser. **129**, 012004 (2008)
46. A.H.C. Neto, F. Guinea, N.M.R. Peres, K.S. Novoselov, A.K. Geim, Rev. Mod. Phys. **81**, 109–162 (2009)
47. A.W.W. Ludwig, M.P.A. Fisher, R. Shankar, G. Grinstein, Phys. Rev. B **50**, 7526–7552 (1994)
48. M. Cheng, P. Fu, X. Chen, X. Zeng, S. Feng, R. Chen, J. Opt. Soc. Am. B **31**, 2325–2329 (2014)
49. X. Li, P. Wang, F. Xing, X.D. Chen, Z.B. Liu, J.G. Tian, Opt. Lett. **39**(19), 5574–5577 (2014)
50. S. Grosche, M. Ornigotti, A. Szameit, Opt. Express **23**, 30195–30203 (2015)
51. N.A.F. Zambale, J.L.B. Sagisi, N.P. Hermosa, Opt. Commun. **433**, 25–29 (2019)
52. W. Wu, S. Chen, C. Mi, W. Zhang, H. Luo, S. Wen, Phys. Rev. A **96**, 043814 (2017)
53. S. Chen, C. Mi, L. Cai, M. Liu, H. Luo, S. Wen, Carbon **149**, 604 (2019)
54. X. Zhou, X. Ling, H. Luo, S. Wen, Appl. Phys. Lett. **101**, 251602 (2012)
55. A.V. Nalitov, G. Malpuech, H. Terças, D.D. Solnyshkov, Phys. Rev. Lett. **114**, 026803 (2015)
56. W.J.M. Kort-Kamp, N.A. Sinitsyn, D.A.R. Dalvit, Phys. Rev. B **93**, 081410 (2016)
57. L. Cai, M. Liu, S. Chen, Y. Liu, W. Shu, H. Luo, S. Wen, Phys. Rev. A **95**, 013809 (2017)
58. T. Tang, J. Li, L. Luo, P. Sun, J. Yao, Adv. Opt. Mater. **6**, 1701212 (2018)
59. X. Zhou, S. Chen, Y. Liu, H. Luo, S. Wen, Proc. SPIE **9167**, 91670I (2014)
60. X. Zhou, Z. Xiao, H. Luo, S. Wen, Phys. Rev. A **85**, 043809 (2012)
61. X. Zhou, J. Zhang, X. Ling, S. Chen, H. Luo, S. Wen, Phys. Rev. A **88**, 053840 (2013)
62. W. Wu, W. Zhang, S. Chen, X. Ling, W. Shu, H. Luo, S. Wen, X. Yin, Opt. Express **26**, 23705–23713 (2018)
63. M. Katsnelson, *Graphene: Carbon in Two Dimensions* (Cambridge University Press, Cambridge, 2012)
64. T. Zhan, X. Shi, Y. Dai, X. Liu, J. Zi, J. Phys.-Condes. Matter **25**, 215301 (2013)

65. H.-S. Yang, S.-Y. Choi, S.-H. Hyun, H.-H. Park, J.-K. Hong, J. Non-Cryst, Solids **221**, 151–156 (1997)
66. D.R. Rolison, B. Dunn, J. Mater. Chem. **11**, 963–980 (2001)
67. M. Schneider, A. Baiker, Catal. Rev.-Sci. Eng. **37**, 515–556 (1995)
68. J.H. Rouse, G.S. Ferguson, J. Am. Chem. Soc. **125**, 15529–15536 (2003)
69. I. Adachi, T. Sumiyoshi, K. Hayashi, N. Iida, R. Enomoto, K. Tsukada, R. Suda, S. Matsumoto, K. Natori, M. Yokoyama, H. Yokogawa, Nucl. Instr. Meth. Phys. Res. A **355**, 390–398 (1995)